Daily Cycle of Precipitation over the Northern Coast of Brazil

SHEILA SANTANA DE BARROS BRITO

Instituto Nacional de Pesquisas Espaciais, Centro de Previsão de Tempo e Estudos Climáticos, São José dos Campos, Brazil

MARCOS DAISUKE OYAMA

Departamento de Ciência e Tecnologia Aeroespacial, Instituto de Aeronáutica e Espaço, Divisão de Ciências Atmosféricas, São José dos Campos, Brazil

(Manuscript received 13 January 2014, in final form 30 July 2014)

ABSTRACT

The daily cycle of precipitation (DCP) in the austral autumn on the northern coast of Brazil (NCB) is examined in detail. The Tropical Rainfall Measuring Mission 3B42 dataset was used to obtain the DCP, and the intradaily variability was measured using the coefficient of variation (CV). The DCP data of the NCB were grouped into five regimes. A new regime was found, called the shore regime. It has a minimum CV, and its cycle shows both continental (late afternoon peak) and oceanic features (morning peak). The landside coastal regime was divided into two areas: a continental coast regime, with very high CV, and an inland coast regime, with clear inland phase propagation. The continental regime was divided into two categories: an inland regime with low and high variability. The Forecast and Tracking of the Evolution of Cloud Clusters (ForTraCC) data were used to relate convective systems (CS) and their processes to the DCP. The following processes are studied for the CS: initiation/dissipation, merge/split, area increase/reduction, and advection. Initiation is more concentrated in time, while dissipation is more distributed. Physical mechanisms that generate initiation can promote area expansion and hence CS merge. By considering a simple parameterization, the time scale of the CS area reduction under environmental conditions that are unfavorable to initiation ranges from 6 to 12 h. Therefore, there is upscaling of the CS in the afternoon and slow decay during the night and morning, which leads to a more uniform cycle inland.

1. Introduction

The daily cycle is a fundamental cycle in the precipitation time series when the data are spaced over a range of hours (e.g., hourly precipitation time series). From the daily cycle of precipitation (DCP), it is possible to know the preferred time of the occurrence and absence of rain, which is useful information for weather forecasting. The DCP features result from specific physical and/or dynamic mechanisms. Both the DCP features (at global and regional levels) and their forcing mechanisms have been extensively studied in the literature (e.g., Janowiak et al. 2005; Bowman et al. 2005; Yang and Smith 2006; Kikuchi and Wang 2008, hereinafter KW08).

In general, the maximum precipitation time depends on the underlying surface involved, whether it is land or ocean. Over land, the diurnal solar heating induces atmospheric instability at the lower levels, which favors the initiation of convective clouds (shallow or deep); therefore, a late afternoon or early evening precipitation maximum is expected. Over the ocean, precipitation generally peaks during the early morning. The different behavior between land and ocean has been noted by many studies using different data sources, such as rain gauge data (Gray and Jacobson 1977; Kousky 1980; Cutrim et al. 2000; Jeong et al. 2011) and satellite-based data (Garreaud and Wallace 1997; Yang and Slingo 2001; Nesbitt and Zipser 2003; Bowman et al. 2005; Silva 2013).

In tropical regions, the DCP can be grouped into four regimes according to KW08: continental, oceanic, seaside coastal, and landside coastal. The DCP of the continental regime has a high amplitude and late afternoon

Corresponding author address: Sheila Santana de Barros Brito, Avenida dos Astronautas, 1758, Bairro Jardim da Granja, 12.227-010, São José dos Campos, SP, Brazil.
E-mail: sheilasbarros@gmail.com

DOI: 10.1175/JAMC-D-14-0029.1

maximum (1500–1800 LST), whereas the oceanic regime has a moderate amplitude and early morning maximum (0600–0900 LST). Coastal regimes occur over the interface between land and ocean. On the landside, the DCP has very high amplitude and there is clear inland phase propagation; on the seaside, the DCP has relatively high amplitude and there is the possibility of offshore phase propagation.

For the northern coast of Brazil (NCB), using rain gauge data (1961–70), Kousky (1980) found that the rate of precipitation depends on the distance from the coastline and the time of day. For example, there is maximum precipitation over the landside coast in the nighttime (2100–0900 LST), and during the daytime, maximum precipitation occurs (1500–2100 LST) over inland regions 100–300 km away from the coast. The nocturnal peak over the coast would be associated with the land breeze process, whereas the inland maximum, especially in the afternoon, would be associated with local convection and inland propagation of coastal squall lines (Cohen et al. 1995).

Janowiak et al. (2005) conducted a global study on DCP and found interesting results for specific regions like South America and, in particular, for the NCB. They showed the existence of different DCP over NCB, from lower to higher variability. The main reason for the afternoon peak over the landside coast was most likely the diurnal heating associated with the sea breeze. The authors found that the maximum precipitation inland propagation produced a nocturnal maximum over areas 500 km away from the coast, ratifying Kousky (1980). From the coast, these systems can reach the Amazon basin in 2 days, according to March–May averages.

Silva (2013) used harmonic analysis to study the DCP over NCB and found that the first two harmonics together explained 60%–90% of the total daily precipitation variance. This indicates that the principal variability modes of the DCP are daily (24 h) and semidaily (12 h) cycles. Furthermore, the results indicate that there are no changes in the timing and location of the maximum precipitation from one season (e.g., January–April) to another (e.g., May–August).

The motivation of this work is the existence of areas in the NCB whose DCP does not fit the regimes proposed by the KW08. For example, the region over the Alcântara Launch Center (ALC; ~2.5°S, ~45°W) would have a landside coastal regime based on the KW08. However, the DCP in the ALC during austral autumn [March–May (MAM)] is fairly uniform, that is, the amplitude is much lower than that expected for the landside coastal regime (Barros 2008). Therefore, taking the regimes defined by the KW08 as a first guess, this work aims at clustering the DCP found over the NCB in a more detailed way. To do this, a simple metric, the coefficient of variation (CV), is used as the main measure of intradaily variability.

As mentioned earlier, the DCP features are understood as resulting from physical and/or dynamic mechanisms. However, the action of a specific mechanism cannot be directly associated with precipitation occurrence because (from the processes sequence perspective) convective systems (CS), which are the main precipitation systems in the tropical region (Velasco and Fritsch 1987; Houze 1993; Wallace and Hobbs 2006; Vila et al. 2008), are the link between mechanisms and precipitation. This distinction is subtle but important because the connection between physical and/or dynamic processes with the life cycle of CS (such as initiation/dissipation, increase/decrease in area, and merge/split) is much more direct. In this work, not only are the variables directly related to precipitation (such as CV, amplitude, and phase) used but also those representing the action and life cycle of CS are used. The CS-related variables are computed from the output of a CS-tracking algorithm known as the Forecast and Tracking of the Evolution of Cloud Clusters (ForTraCC; Vila et al. 2008) and are analyzed in the various DCP regimes. This type of analysis approximates CS studies (e.g., Garreaud and Wallace 1997; Machado et al. 1998; Laurent et al. 2002; Barbosa et al. 2006; Gonçalves 2013) to DCP studies (e.g., Janowiak et al. 2005, KW08). Furthermore, this allows for singling out the main processes of the CS life cycle that shapes the DCP as well as for a discussion on the physical and/or dynamic mechanisms associated with these processes.

This work is organized as follows: The data used are described in section 2. The methods are presented in section 3. The results of the DCP regimes over the NCB using precipitation data (rainfall estimates) are shown in section 4. The daily cycle of CS occurrence for the various regimes using ForTraCC outputs is found in section 5, and the concluding remarks are given in section 6.

2. Data

a. Precipitation

Precipitation estimates from version 6 of the Tropical Rainfall Measuring Mission (TRMM) 3B42 data product are used. The dataset is based on infrared and microwave sensors as well as radiometers. The technique is called TRMM Multisatellite Precipitation Analysis (TMPA) (Huffman et al. 2007). The time period was

from 1 January 1998 to 31 March 2010. The spatial resolution was 0.25° × 0.25°, and temporal resolution was 3 h. The TRMM data refer to the average precipitation rate on a 3-h interval centered at the following times: 0000, 0300, 0600, ... , 2100 UTC. The data were available from 50°N to 50°S and for all longitudes.

A preliminary comparison between TRMM and in situ, collected data was carried out by Brito (2013) for several meteorological stations within NCB. The results showed that the TRMM 3B42 data underestimate the precipitation magnitude but the DCP phase is well represented. The latter result is in line with regional validation studies of the TRMM 3B42 data (e.g., Zhou et al. 2008), which show that the phase bias reported by several authors (Janowiak et al. 2005; KW08; Sapiano and Arkin 2009) might not be found on a regional level. Therefore, the TRMM data would be useful to study the DCP of the NCB.

b. *Convective systems*

The output of the ForTraCC algorithm for the period between June 2004 and April 2011 is used. ForTraCC identifies and tracks the CS through its life cycle. The first version of ForTraCC was developed by Machado et al. (1998), and the final version, which is currently operational at Centro de Previsão de Tempo e Estudos Climáticos/Instituto Nacional de Pesquisas Espaciais (CPTEC/INPE), was coded and validated by Vila et al. (2008). The method uses brightness temperature from the Geostationary Operational Environmental Satellite as input. The CS are detected using a threshold of 235 K, and 210 K is used to define the convective cells. The tracking is based on area superposition (>150 pixels or 2400 km^2) on successive images. The CS split and merge are also considered by the algorithm.

3. Methods

a. *Daily cycle of precipitation*

The daily average rainfall is computed as $\overline{x} = \sum_{i=1}^{i=n} x_i/n$, where $n = 8$ and $i = 1$, which corresponds to 0000 UTC, $i = 2$ corresponds to 0300 UTC, and so on; x refers to the TRMM precipitation data. The standard deviation s and coefficient of variation CV are calculated using the following expressions:

$$s = \sqrt{\frac{\sum_{i=1}^{i=n} (x_i - \overline{x})^2}{n-1}} \quad \text{and} \quad \text{CV} = 100\frac{s}{\overline{x}}, \tag{1}$$

where high (low) CV value is related to higher (lower) DCP variability.

b. *Uniformity of the DCP*

The concept of a confidence interval for a population proportion is used to evaluate the DCP uniformity (Spiegel 1978). For theoretical purposes, a uniform DCP would correspond to the following probability density function:

$$f(x) = \begin{cases} 1/8, & x = 1, 2, \ldots, 7, 8 \\ 0, & \text{otherwise} \end{cases}. \tag{2}$$

It follows that $\sum_{i=1}^{i=8} f(i) = 1$. The goal is to obtain a range for $f(x)$ for which the series can be considered uniform (at a certain level of confidence).

The sample size n is the number of days used to obtain the DCP. In austral autumn (MAM), 12 yr of data correspond to 1080 days (90 days × 12 yr). According to Spiegel (1978), to apply the confidence interval for the ratio $p = 1/8$, two conditions must be met: $np \geq 5$ and $n(1-p) \geq 5$. Because $np = 1080/8 = 135 \geq 5$ and $n(1-p) = 1080(1-1/8) = 1080 \times 7/8 = 945 \geq 5$, the two conditions are met. Therefore, the confidence interval at a $(1-\alpha)$ confidence level is $p \pm e_0$, where

$$e_0 = z_{\alpha/2}\sqrt{\frac{p(1-p)}{n}}, \tag{3}$$

and $z_{\alpha/2}$ is the tabulated value for the normal distribution.

By Eq. (3), the value of e_0 at a significance level of 1% is 0.259 64. Therefore, the confidence interval for a uniform DCP is (1/8 + 0.259 64; 1/8 − 0.259 64). We consider a simple DCP that consists of the first harmonic with a null phase added to the mean, that is, $y_t = \overline{y} + A\sin(2\pi t/T)$, where $\overline{y}$ is the series mean, A is amplitude, T is the period, and the variance s^2 and standard deviation s of y_t are $s^2 = A^2/2$ and $s = \sqrt{s^2} = (\sqrt{2}/2)A$ (Wilks 2006). The CV is $\text{CV} = (\sqrt{2}/2)(A/y)$. While a uniform DCP has a variation given by $1/8 - e_0 \leq 1/8 \leq 1/8 + e_0$, the simple DCP has a variation given by $\overline{y} - A \leq \overline{y} \leq \overline{y} + A$. The latter could be rewritten as

$$\begin{aligned} \overline{y} - A \leq \overline{y} \leq \overline{y} + A &\Rightarrow 1 - \frac{A}{\overline{y}} \leq 1 \leq 1 + \frac{A}{\overline{y}} \\ &\Rightarrow \frac{1}{8} - \frac{A}{8\overline{y}} \leq \frac{1}{8} \leq \frac{1}{8} + \frac{A}{8\overline{y}}. \end{aligned} \tag{4}$$

Therefore, the simple DCP can be regarded as uniform if $e_0 \geq A/8\overline{y}$. If $e_0 = A/8\overline{y}$, we obtain the following

$$e_0 = \frac{A}{8\overline{y}} = \frac{1}{8}\frac{A}{\overline{y}} = \frac{1}{8}\frac{2}{\sqrt{2}}\underbrace{\frac{\sqrt{2}}{2}\frac{A}{\overline{y}}}_{\text{CV}}, \tag{5}$$

and then

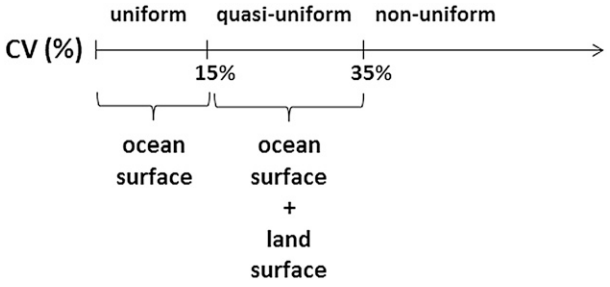

FIG. 1. The CV thresholds for the uniform, quasi-uniform, and nonuniform daily cycles.

$$e_0 = \frac{1}{8}\frac{2}{\sqrt{2}}\mathrm{CV} \Rightarrow \mathrm{CV} = 4\sqrt{2}e_0, \tag{6}$$

using the e_0 value from Eq. (3) in Eq. (6), $\mathrm{CV} = 4\sqrt{2} \times 0.259\,64 \Rightarrow \mathrm{CV} \approx 15\%$. Therefore, the CV values between 0% and 15% indicate regions with a uniform DCP.

The DCP is defined here as quasi uniform if the amplitude (maximum minus minimum) is not greater than the average. Applying this definition to the simple DCP, we have $\overline{y} - A \geq (1/2)\overline{y}$. Using Eq. (5), it follows that

$$\overline{y} - \frac{1}{2}\overline{y} \geq A \Rightarrow \overline{y}\left(1 - \frac{1}{2}\right) \geq A \Rightarrow \frac{\sqrt{2}}{2}\frac{A}{\overline{y}} \leq \frac{\sqrt{2}}{2}\frac{1}{2} \Rightarrow \mathrm{CV} \leq \frac{\sqrt{2}}{4} \cong 35\%. \tag{7}$$

Therefore, the range $15\% < \mathrm{CV} \leq 35\%$ indicates regions with a quasi-uniform DCP. Figure 1 summarizes the thresholds based on the CV to delimit regions with a uniform daily cycle ($\mathrm{CV} \leq 15\%$), a quasi-uniform daily cycle ($15\% < \mathrm{CV} \leq 35\%$), and a nonuniform daily cycle ($\mathrm{CV} > 35\%$).

The harmonic analysis used to study DCP is based on Wilks (2006). The amplitude, phase, and fraction of variance for each harmonic are calculated.

c. *Daily cycle of convective systems*

All of the CS detected by ForTraCC from the initial position belonging to a region between latitudes 32.625° and 12.875°N and longitudes 82.625° and 27.125°W were selected. The area encompasses the entire continent of Brazil. A larger area (than the NCB) is used to avoid the problem of edge. Spurious CS are excluded by a filter. The filter is performed according to the average propagation speed of the system calculated by the distance (from the starting to the ending position) and the system duration.

The CS that occur in austral autumn between 2005 and 2010 are listed in time order for every 15 min. Systems occurring 1.5 h before and 1.5 h after the following times (0000, 0300, 0600, . . . , 2100 UTC) were selected. To quantify the occurrence of the CS, two variables were used: frequency (FREQ) and convective area fraction (FRAC). For a horizontal area of 2.5° × 2.5°, during a 3-h time interval, the FREQ is the monthly average number of CS that affects the area; the FRAC is the average area fraction covered by CS.

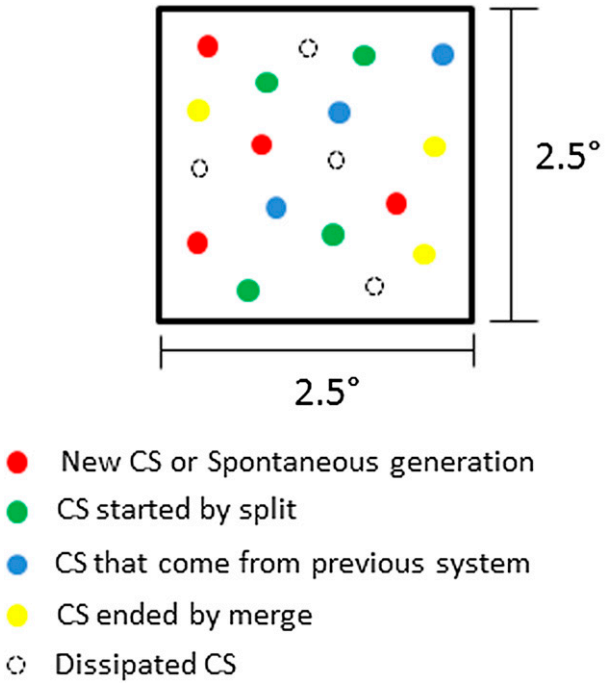

FIG. 2. Schematic diagram illustrating the CS initiation.

Figure 2 illustrates the processes of the CS life cycle according to the ForTraCC data. It can represent an area of 2.5° × 2.5° for 1500 UTC, for example. This means that all of the CS present between 1330 and 1630 UTC are plotted. In the example, four systems started by spontaneous generation (red), three systems ended by merge (yellow), and four systems formed by split (green).

The FREQ and FRAC are obtained for the following four CS processes:

1) initiation ($\overline{f}_{\mathrm{initiation}}$) corresponds to new or spontaneous generation systems by ForTraCC (first family member),
2) dissipation ($\overline{f}_{\mathrm{dissipation}}$) corresponds to last family members, in other words, the last time that CS is observed by ForTraCC,
3) merge indicates systems that join each other to form a single system, and
4) split indicates systems that are separated.

The intradaily variability of these features (CS occurrence, initiation, dissipation, merge, and split) is evaluated by calculating the CV.

The FRAC temporal variations result from three processes: CS net initiation (initiation minus dissipation), CS net area expansion (CS area increase minus decrease), and zonal advection (because the CS propagates zonally from east to west). Therefore,

$$\Delta f = (f_{\text{initiation}} - f_{\text{dissipation}}) + (f_{\text{source}} - f_{\text{sink}}) + \Delta f_{\text{advection}}, \quad (8)$$

where the first term is the temporal difference in the FRAC ($\Delta f = f_t - f_{t-1}$), the second term is the gain (loss) associated with the FRAC initiation (dissipation), the third term is gain (loss) associated with a FRAC increase (decrease), and the fourth term is a gain–loss associated with CS zonal advection. Only the zonal component is considered because the CS moves generally eastward over the NCB, according to Machado et al. (1998).

The first right side term of Eq. (8) is obtained as $\overline{f}_{\text{initiation}}$ minus $\overline{f}_{\text{dissipation}}$. The third term is obtained as follows:

$$\Delta f_{\text{advection}} = \frac{\Delta t}{2\Delta x}|u|(f_{i-1} - f_{i+1}). \quad (9)$$

In this expression, $\Delta t = 3\,\text{h}$, $\Delta x = 0.5°$, and $|u| \approx 8\,\text{m s}^{-1} \approx 0.26°\,\text{h}^{-1}$; an estimation to $(\Delta t/2\Delta x)|u|$ is $(\Delta t/2\Delta x)|u| \approx (3 \times 0.26)/(2 \times 0.25) \cong 1.5$. This value is regarded as constant for simplicity. The second term is calculated as residue:

$$(f_{\text{source}} - f_{\text{sink}}) = \Delta f - (f_{\text{initiation}} - f_{\text{dissipation}}) - \Delta f_{\text{advection}}. \quad (10)$$

To evaluate the terms of the net area expansion, the area increase f_{source} is parameterized as a function of the CS initiation:

$$f_{\text{source}} = \alpha \Delta t \overline{f}_{\text{initiation}}, \quad (11)$$

where α is a tuning parameter (also considered constant for simplicity). The area reduction (f_{sink}) is therefore calculated as residue:

$$f_{\text{sink}} = \Delta f - (f_{\text{initiation}} - f_{\text{dissipation}}) - \Delta f_{\text{advection}} - f_{\text{source}}. \quad (12)$$

A simple way to represent the CS area reduction is to consider the FRAC exponential decay when there are no atmospheric mechanisms favorable to the FRAC increase:

$$\frac{df}{dt} = -\frac{f}{\tau}. \quad (13)$$

In this expression τ is an *e-folding time* parameter, a time scale measure of the decay process. An estimate of this parameter can be obtained from the following expression:

$$\tau = \frac{\Delta t f_{t-1}}{f_{\text{sink}}}. \quad (14)$$

4. Daily cycle of precipitation

a. Intradaily variability

The DCP over tropical South America in austral autumn is shown in Fig. 3. A sharp precipitation increase takes place on the continent during midafternoon (1800 UTC) over two regions: the landside coast (region I) and central Amazonia (region III). For both regions, this increase would be the result of diurnal heating forcing and, for region I, also due to sea breeze circulation (Janowiak et al. 2005). Between regions I and III, there is a belt of local precipitation minima (region II). Until evening (2100 UTC), the precipitation continues increasing over regions I and III, and the precipitation maxima propagate slightly westward. During the night and morning (from 0000 until 1200 UTC), the precipitation decreases, and the afternoon precipitation maximum over region I progressively weakens while propagating inland toward region III. The inland propagation of the precipitation maximum from the landside coast is known as phase propagation (Rickenbach 2004; KW08), and it resembles the inland propagation of squall lines (Alcântara et al. 2011). At midday (1500 UTC), the weak precipitation maximum over central Amazonia, which could be traced back to the landside coast maximum from the previous afternoon, is the preferential area for precipitation reintensification in the following afternoon hours; therefore, region III is also referred to as a reintensification region. Over the seaside coast, the precipitation slowly increases during the late night and morning (from 0600 to 1200 UTC) and then decreases during the early afternoon (from 1500 to 1800 UTC). This behavior is a result of land breeze circulation (Kousky 1980; Teixeira 2008). Over oceanic areas far from the coast, precipitation is mostly constant throughout the day.

The intradaily variability over tropical South America, measured by the CV, is shown in Fig. 4. To focus on humid lowland tropical regions, areas with average precipitation below $0.1\,\text{mm h}^{-1}$ (e.g., the driest portions of Northeast Brazil) or heights above 500 m are filtered out.

Initially, the intradaily variability shows maximum values over the landside coast and decreases both

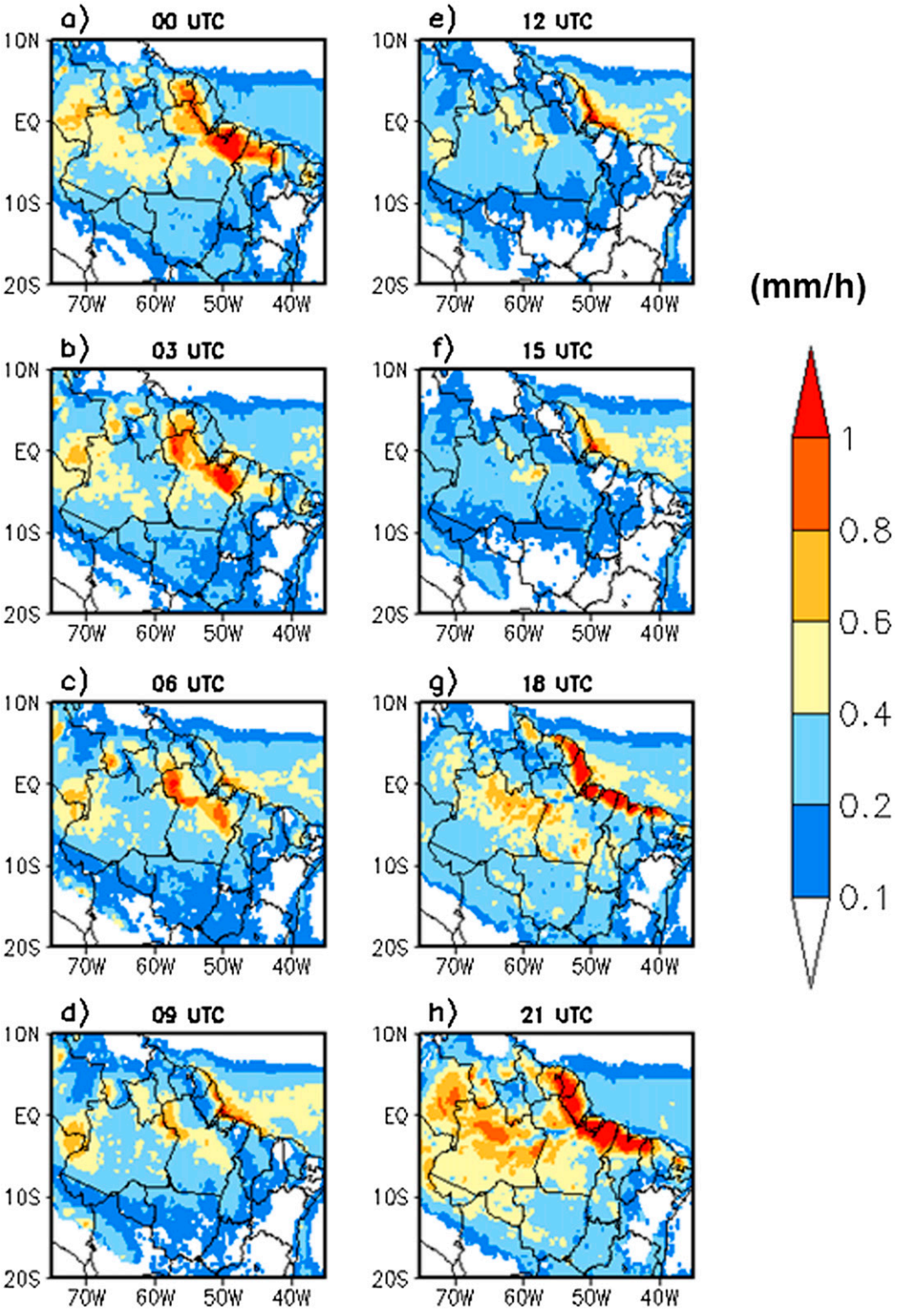

FIG. 3. Daily cycle of precipitation (mm h^{-1}) over tropical South America in austral autumn considering the TRMM data from 1 Jan 1998 until 31 Mar 2010: (a)–(h) 0000–2100 UTC in 3-h increments.

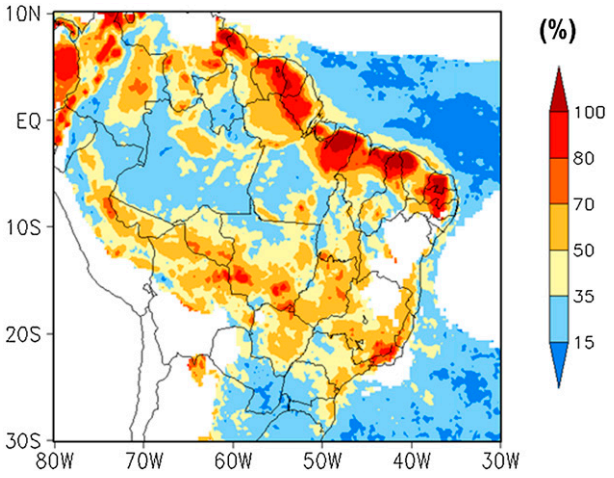

FIG. 4. Intradaily variability over tropical South America measured by the CV (%). Areas with an average precipitation $< 0.1\,\text{mm}\,\text{h}^{-1}$ or heights $> 500\,\text{m}$ are filtered out.

offshore and inland. Over the ocean, the variability is low–moderate (nonuniform cycle) along the seaside coast and decreases offshore to become very low (uniform cycle). For the continent, the variability is very high over the landside coast (region I) and decreases inland to a low level (quasi-uniform cycle). This general pattern resembles the location of the DCP regimes of the KW08 for tropical South America (Fig. 10 of KW08). For the ocean, the two regimes of KW08 (oceanic and seaside coastal regimes) are suitable to group the different intradaily variability features. For the continent, the two regimes of the KW08 (continental and landside coastal regimes) are able to represent the general pattern of intradaily variability, but some important regional details are not discerned by them. Therefore, new regimes for the continent are proposed here.

The minimum CV values are found between the seaside and landside coast, over a narrow strip (width of ~1°) along the shore between 50° and 40°W. Therefore, over this strip, the transition of the variability (from ocean to land) is not monotonic, but passes through a minimum of CV. This behavior is regarded as a new regime—the shore regime—and it was noticed previously for specific locations, such as the ALC (Barros 2008). To illustrate the features of the shore regime, the DCP of specific locations is shown in Fig. 5a. From A to C, the cycle changes from uniform to quasi uniform, as the maximum at 1200 UTC becomes more pronounced. Point D corresponds to the shore regime. The cycles over C and D are similar, except at 2100 UTC when an incipient maximum over D is found. Therefore, the cycle over D may be viewed as a predominantly seaside coastal cycle to which an incipient afternoon maximum is added.

The landside coastal regime of the KW08 covers the continental coastal area with high variability. Instead of belonging to a single regime, the DCP features over this area could be grouped in two distinct regimes: in the first (the continental coast regime), which occurs over regions closer to the shore, the variability was very high (CV > 70%) and the maximum CV value was found; in the second (the coast–inland regime), the variability was high (50% < CV < 70%), the CV decreased inland, and phase propagation took place. To illustrate the features of these two regimes, the DCP of specific locations are shown in Fig. 5b. Point A is over the landside coast (region I) and represents the continental coast regime. From A to D, there is phase propagation, maximum decay, and the cycle changes from nonuniform to quasi uniform. Point D is in region II, which is a region of low variability that lies between regions I and III. Another interesting feature is the minimum precipitation inland increase: in A, it was almost zero, and from B to D, it increased to approximately $0.3\,\text{mm}\,\text{h}^{-1}$. The cycle over B represents the coast–inland regime.

Far from the coast, core areas with moderate/high variability (35% < CV < 70%) are embedded in the large inland areas with low variability (CV < 35%). These core areas are not randomly placed, but are organized as a belt parallel to the coast that corresponds to region III. Therefore, instead of considering a single continental regime, such as proposed by KW08, it would be more precise to depict the regimes over the continent as a sequence of alternating low (e.g., region II) and moderate–high (e.g., region III) variability regimes.

The results from a harmonic analysis of DCP are shown in Fig. 6. In general, over high intradaily variability areas, the variance is dominated by the first harmonic (Fig. 6a), and the first harmonic phase provides information about when the precipitation maximum occurs (Fig. 6b). The phase pattern clearly shows an inland propagation of the maximum precipitation (phase propagation). On the oceanic side, offshore phase propagation is found over the seaside coast of Ceará State, where phase propagation related to the land-breeze coast is also found from wind data at 1000 hPa (D. C. Souza 2013, personal communication; Teixeira 2008).

The vector and magnitude of the first harmonic phase gradient are shown in Fig. 7. (Hereinafter the gradient magnitude will be referred to as GRAD.) For the regions where the first harmonic dominates, assuming that the propagation of precipitation maxima and CS is related, GRAD is inversely proportional to the CS propagation velocity. Unrealistic low (high) velocities lead to high (low) GRAD. Therefore, phase propagation is likely to occur over regions with intermediate values of GRAD, such as a few hours per degree. Under this criterion for

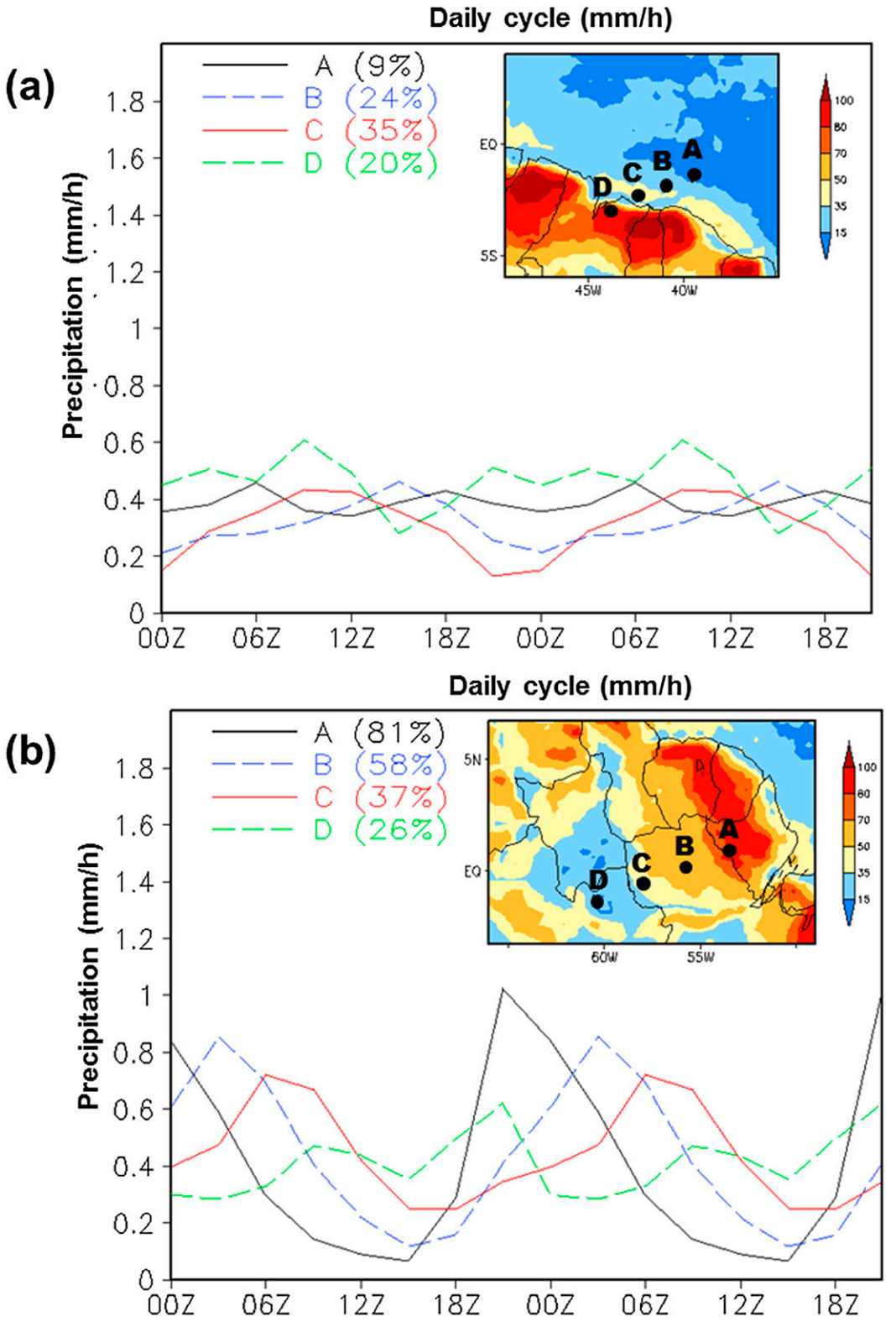

FIG. 5. Daily cycle at specific locations: (a) the transition from the oceanic to the shore regime and (b) the various continental regimes.

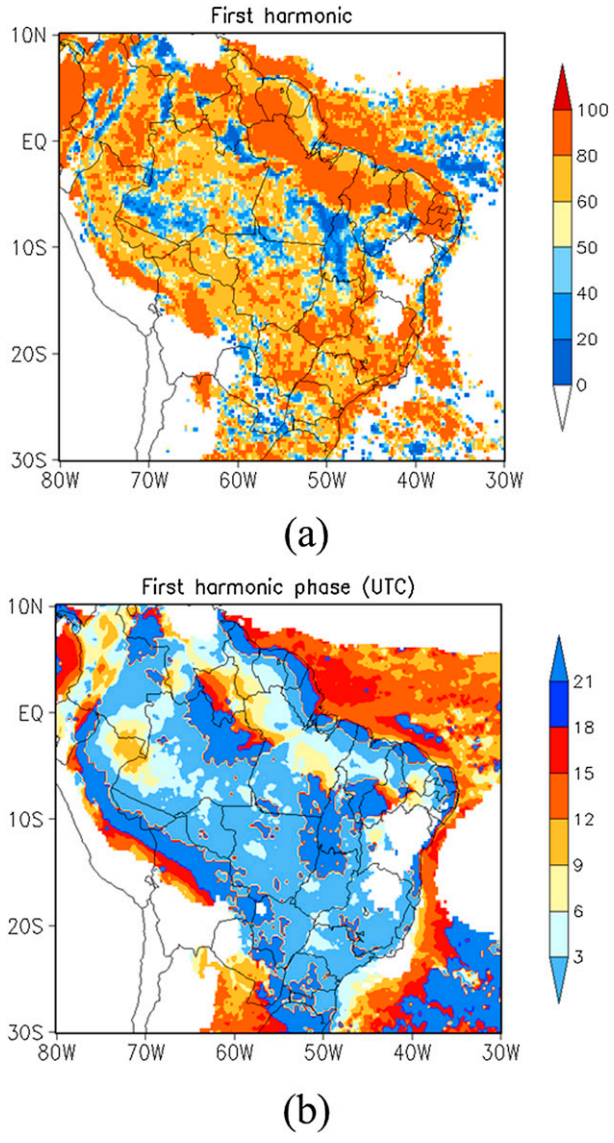

FIG. 6. Results of the harmonic analysis: (a) the variance of the first harmonic and (b) the first harmonic phase.

the continent, the phase propagation generally lies between the westward to southward directions (southwestward on average) and occurs over the landside coast (region I) and the reintensification region (region III). For the ocean, offshore phase propagation is found over some seaside coastal areas (e.g., over the Ceará seaside coast). In general, phase propagation is an important feature over transition zones between eastern higher and western lower variability regions.

b. Precipitation regimes

The occurrence of the DCP regimes proposed here are shown in Fig. 8, and the identification criteria for each regime are given in Table 1. For a given region, the four inputs are surface type (land/ocean), (minimum) distance to the coastline, CV, and first-order GRAD. The output is one of the seven regimes or may be "undefined," which means that the input information does not meet the criteria for all regimes, and therefore the region lies in a transition zone between the regimes. Coastal regimes (types 2–4) occur within 2° from the coastline. For the inland regimes (types 6 and 7), a distance greater than 7° from the coastline is needed. This condition is based on the idea that inland regimes are not directly influenced by phase propagation related to the late afternoon precipitation maximum over the landside coast; a threshold of 7° is approximately the distance of the weak precipitation maximum at midday (1500 UTC) in central Amazonia from the coastline (Figs. 3f, 6b).

In the ocean, there is a large transition zone between the oceanic (type 1) and seaside coastal (type 2) regimes. Over this zone, offshore phase propagation could occur (Fig. 6b). The KW08 considers that the transition zone belongs to the seaside coastal regime, but here we restrict the type 2 regime to only the seaside coastal areas with higher variability. The narrower extension of the type 2 regime is consistent with the idea that the land breeze is weaker than the sea breeze mechanism (Kousky 1980; Teixeira 2008).

On the continent, the landside coastal regime of the KW08 is divided into three areas: shore regime (type 3), continental coast regime (type 4), and coast–inland regime (type 5). The shore regime has the lowest variability and its cycle presents both oceanic and continental features. The continental coast regime is found over region I, where the global precipitation maximum takes place, variability is very high, and the precipitation minimum is almost zero. In the coast–inland regime, clear phase propagation takes place, variability decreases inland but remains high, and the precipitation minimum increases. The transition zone between type 5 and the inland regimes corresponds to region II, where variability is low. Phase propagation is also found over region II, but it is not so clear because the first harmonic is dominant only in some parts of the region.

In the continental interior, that is, far from the coastline, daily variability takes place in two distinct modes: lower and higher variability inland regimes (types 6 and 7, respectively). In type 7, phase propagation may occur (Fig. 7); that is, phase propagation is a process that is found not only over the coast–inland area but also inland. Type 7 is found over region III (reintensification region).

There are differences between the TRMM algorithms over oceanic and continental regions (Turk et al. 2008; Sapiano and Arkin 2009). This indicates that there are uncertainties related to the existence and location of the

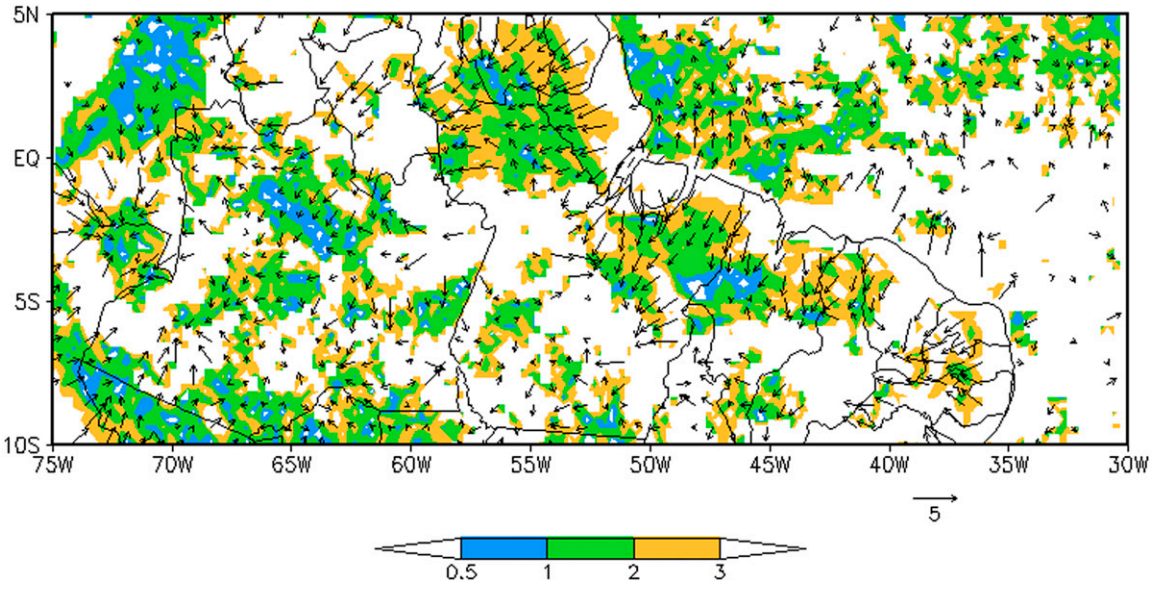

FIG. 7. First harmonic phase gradient. The vectors indicate the direction, and the shades indicate magnitude [GRAD; h $(°)^{-1}$].

type 3 regime because it is located along the transition between the ocean and continent. This issue is ameliorated by the results of Brito (2013), who found that the DCP is reasonably well reproduced by the TRMM 3B42 data (when compared with the DCP based on rain gauge collected data) for several stations within NCB, including few close to the shore (cf. section 2a). Furthermore, the usefulness of the TRMM 3B42 data for coastal

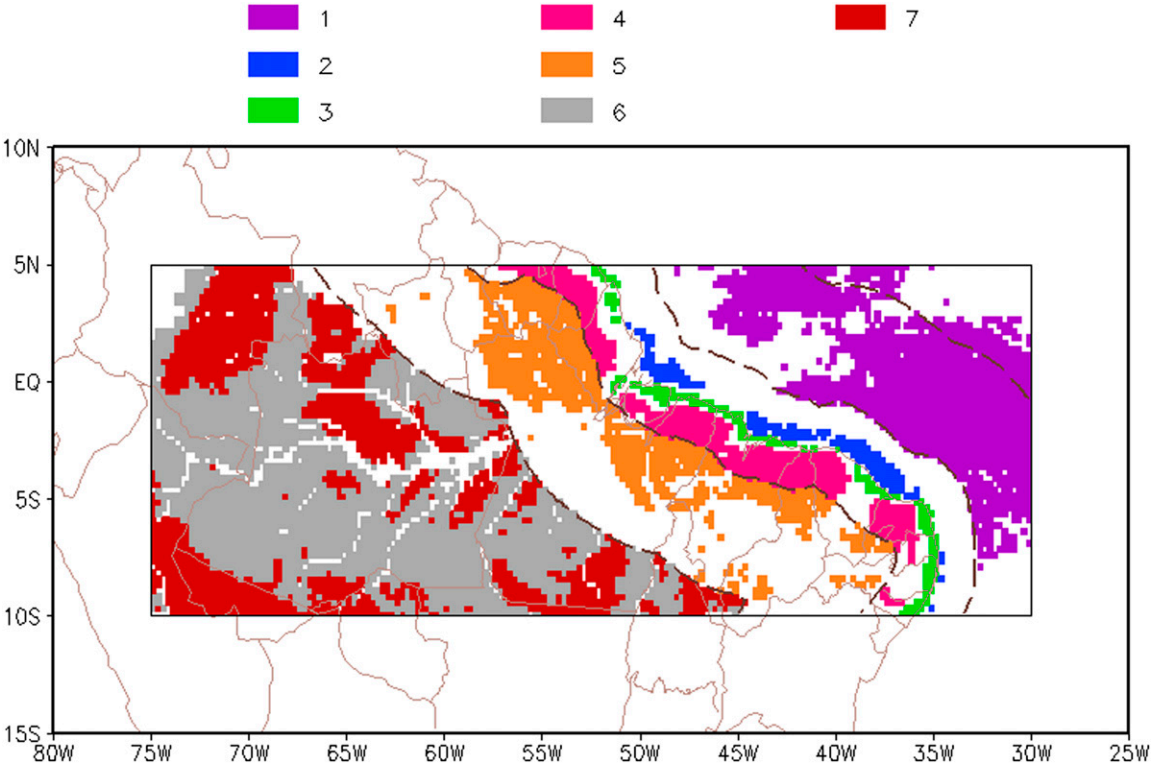

FIG. 8. Daily cycle regimes proposed to the NCB. The dashed lines indicate a distance of 2°–7° to shore. Areas with heights above 500 m, rivers, and lakes are filtered out. The numbers in the color key refer to the regimes' types given in Table 1: 1) oceanic regime, 2) seaside coastal regime, 3) shore regime, 4) continental coast regime, 5) coast–inland regime, 6) low-variability inland regime, and 7) high-variability inland regime.

TABLE 1. Identification criteria for each regime proposed to the NCB.

Type	Regime	Surface	Distance from coast (°)	CV (%)	GRAD [h (°)$^{-1}$]
1	Oceanic	Ocean	>2	≤15	—
2	Seaside costal	Ocean	≤2	≥35	—
3	Shore	Land	≤2	≤35	—
4	Continental coast	Land	≤2	≥70	—
5	Coast–inland	Land	>2 and ≤7	≥50	>1 and <4
6	Low-variability inland	Land	>7	<35	—
7	High-variability inland	Land	>7	≥35	—

areas has been assumed for specific regions (e.g., Mao and Wu 2012; for the Asian monsoon region) because validation for all tropical coastal areas is not found. In spite of these supporting aspects, the features of the type 3 regime should be further confirmed by using other datasets.

The main effects of phase propagation on the DCP—intradaily variability (CV) decrease and minimum precipitation increase (e.g., type 5 regime)—can be obtained from the idealized representation shown in Fig. 9a. It is assumed that the precipitation cycle is the result of adding two functions: a cosine function that represents the characteristic daily cycle over the continent (solid line), and a Gaussian function that represents the additional precipitation due to phase propagation (dashed and dotted lines). When the Gaussian function is centered at 1800 UTC (dashed line with squares), the two maxima are added, the highest variability cycle is found (CV = 100%), and the cycle (as well as the CV value) resembles the average cycle of the type 4 regime. Inland phase propagation from the coast is represented by Gaussian functions centered in the subsequent hours (2100, 0000, 0300, and 0600 UTC) with decreasing amplitude. The resulting pattern is similar that the found in Fig. 5b. Phase propagation leads to a bimodal cycle (0600 UTC), and the CV decreases from 100% to 30% (quasi-uniform cycle). The minimum precipitation increases from 0300 UTC; for example, at 0600 UTC, the minimum is similar to the maximum and resembles the cycle found over region III.

The existence of a shore regime (type 3) with the lowest variability (minimum CV) can be understood from the idealized representation shown in Fig. 9b. It is assumed that the precipitation cycle over the shore is the weighted average of two functions: a cosine function (solid line) that represents the daily cycle of type 2 (early morning maximum and late afternoon minimum) and a Gaussian function centered at late afternoon (dotted line with dash) that represents the daily cycle of type 4. By considering a weight of 75% for the cosine function and 25% for the Gaussian (line L1 in Fig. 9b), the CV is at a minimum (19%), and the cycle is bimodal with similar magnitude maxima values in the early morning (oceanic feature) and late afternoon (continental feature)—this resembles a type 3 average cycle.

5. Daily cycle of convective systems

a. *Occurrence of convective systems*

The daily cycle in the FRAC is shown in Fig. 10, and the daily cycle of the FREQ is similar to the FRAC's (not shown). Both cycles are similar to the DCP (Fig. 3). The temporal linear correlation between the precipitation and the FREQ–FRAC cycles is, in general, high ($r > 0.9$, not shown), and the precipitation intradaily variability spatial pattern is accurately reproduced by the FREQ–FRAC (Fig. 11, not shown to the FREQ). However, the precipitation spatial pattern is better reproduced by the FRAC. For instance, between 2100 and 0000 UTC, the precipitation maximum over the reintensification region in central Amazonia (region III) does appear in the FRAC field, but does not appear in FREQ's. In spite of these differences, the main features of the DCP described previously are also found in the FREQ and FRAC cycles.

The similarity between the daily cycles of precipitation and the FREQ–FRAC is an important result because it proves that physical–dynamic mechanisms are connected to precipitation through a CS occurrence. This connection has usually been implicitly assumed (e.g., Garreaud and Wallace 1997; Bowman et al. 2005; Gonçalves 2013), and here it is explicitly shown. It also indicates that CS-related processes shape the different precipitation regimes.

b. *Frequency of convective systems initiation, dissipation, merge, and split*

The daily cycle of frequency of the CS net initiation (initiation minus decay) and net split (split minus merge) are shown in Figs. 12 and 13, respectively. In general, the frequency values for net initiation and net split have the same order of magnitude of FREQ, but opposite signs. At first order, the intradaily variability of the net initiation is higher (lower) over the continent (ocean), ratifying Gonçalves (2013).

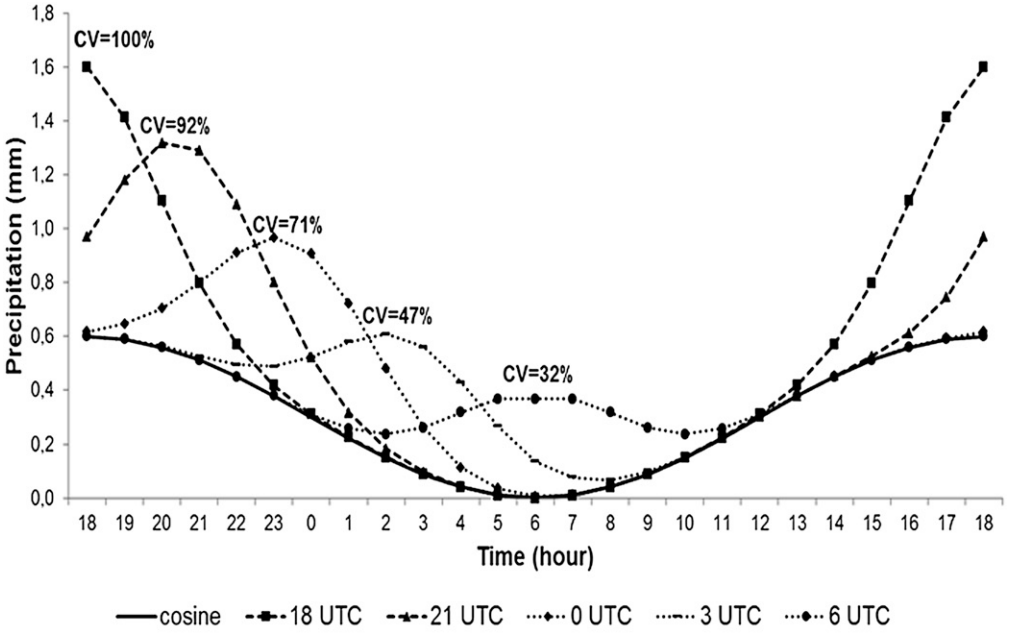

(a)

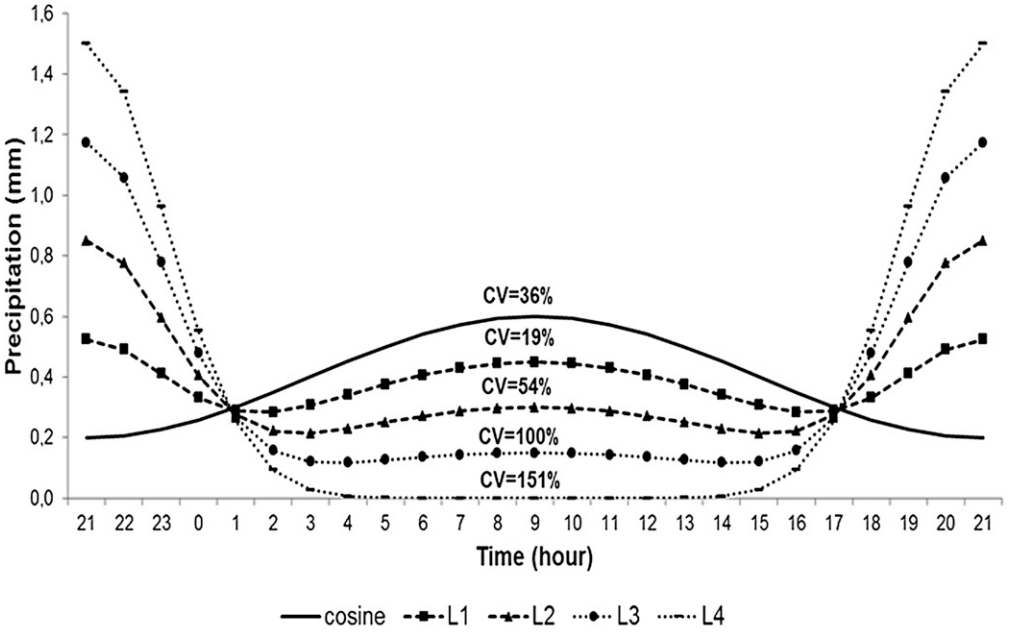

(b)

FIG. 9. Idealized representation to illustrate (a) the effects of phase propagation and (b) the existence of the shore regime with lowest variability. In (a), the daily cycle over land is expressed by adding a cosine function (solid line) that represents the characteristic daily cycle over the continent and a Gaussian function that represents the precipitation due to phase propagation. Dashed line with closed squares represents the daily cycle for the Gaussian function centered at 1800 UTC, dashed line with closed triangles represents the cycle at 2100 UTC, and so on. In (b), the precipitation cycle over the shore (L1, L2, or L3) is regarded as the weighted average of two functions: a cosine function that represents the daily cycle of type 2 (seaside coastal regime; solid line) and a Gaussian function centered at late afternoon that represents the daily cycle of type 4 (continental coast regime; dotted line with dash; L4). Over the shore, from the seaside to the continental coast, the precipitation cycle would change from L1 to L3.

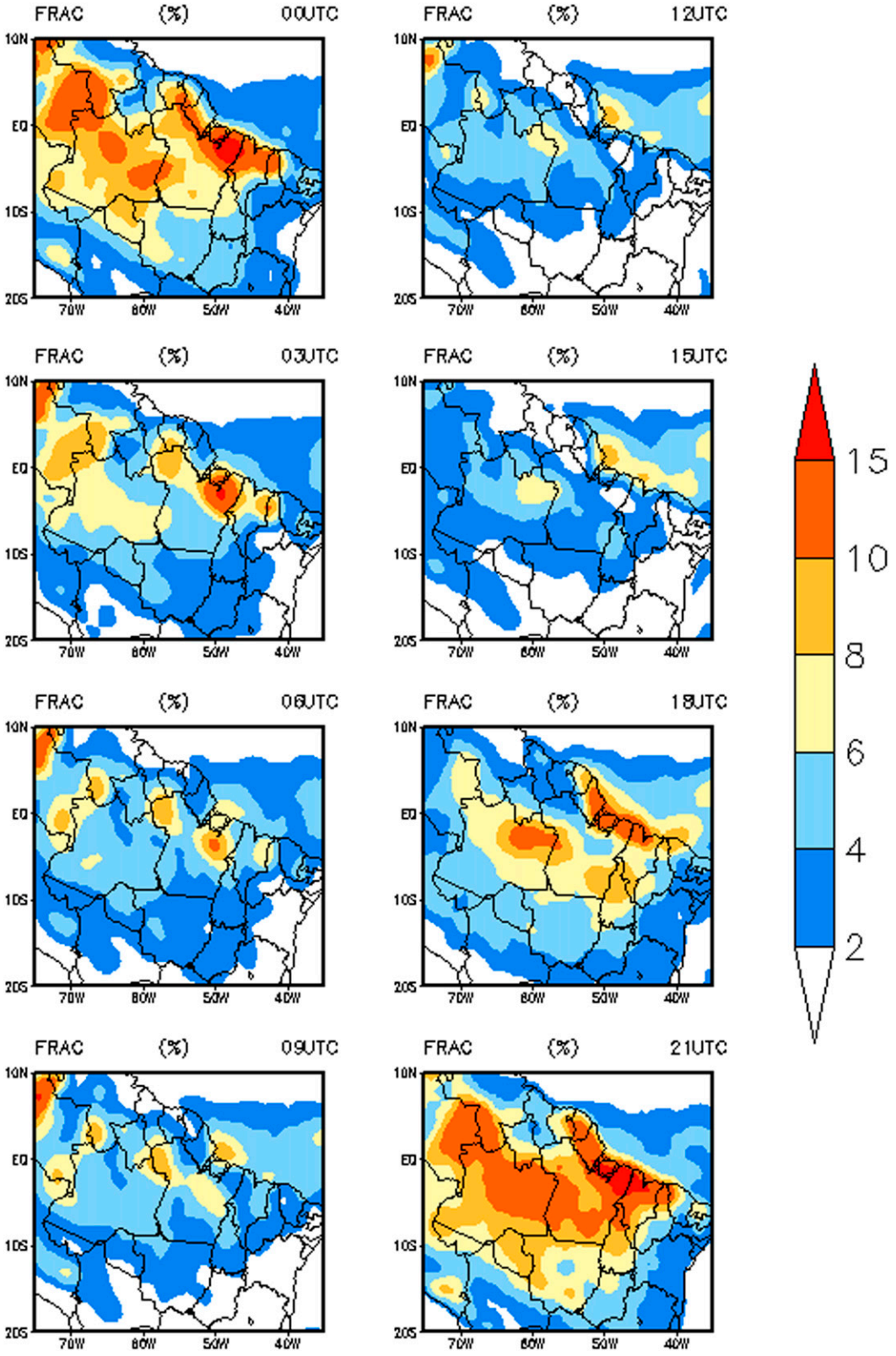

FIG. 10. Daily cycle of the average convective area fraction covered by the CS (FRAC).

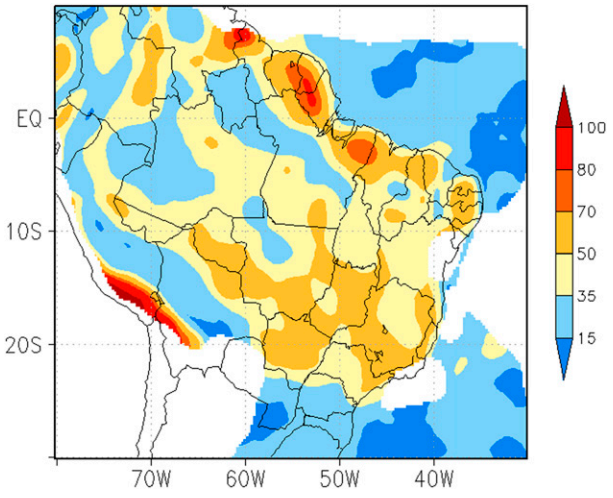

FIG. 11. Coefficient of variation for the FRAC.

Over the continent, there is high similarity between the daily cycles of initiation and merging and of the decay and split. This suggests, on the one hand, that the same physical mechanisms that favor CS initiation may be important to CS area expansion and the consequent merge occurrence; on the other hand, CS weakening involves two processes that act concurrently: a split in the larger CS (cf. Machado and Rossow 1993) and the decay of the smaller ones.

While the occurrence of the net initiation–merge is concentrated on the afternoon (1800 UTC), the occurrence of the net dissipation/split is spread over the remaining hours (night and morning) and exhibits a maximum in the early night (0000 UTC). This behavior explains the higher (lower) intradaily variability of the initiation/merge (dissipation/split), as shown in Fig. 14. The primary physical mechanism that favors net initiation/merge would be diurnal solar heating. When this mechanism is absent (night) or incipient (morning), a CS decay in the form of net dissipation–split prevails.

During the afternoon, net initiation was not concentrated in regions I or III, as the FRAC fields would suggest, but was widespread over the inland areas. In these hours, the distinction between coastal and inland areas could be noticed in the merge field, which showed a maximum over region I (Figs. 13; 2100 UTC). This behavior could result from the sea breeze. During the night and morning, although a net dissipation/split was found, there was still initiation/merge at a smaller magnitude [this result ratifies the pattern found in Fig. 4.5 of Gonçalves (2013)]. The occurrence of the initiation–merge during the night and morning could be the result of nocturnal convection processes, such as those induced by low-level jets or autopropagation processes related to convective systems organized at larger scales (Cotton and Anthes 1989).

Over the ocean, the lower (higher) initiation in the diurnal (nocturnal) period agrees with Fig. 4.5 in Gonçalves (2013). In relation to the split/merge process, a higher net split is found between 1800 and 2100 UTC.

c. *Convective area FRAC budget*

The FRAC changes over time because of three processes: a net initiation (CS initiation minus CS dissipation), a net area expansion (area increase of CS minus a decrease), and zonal advection (because, on average, the CS propagates westward). The daily cycle of the FRAC temporal variation, as well as the variations due to the three processes, are shown in Fig. 15. The variation due to net expansion is calculated as residue.

At first order, the dominant process for the temporal variation in the FRAC is the net area expansion. The advection and net initiation processes are important for some regions/hours and contribute to shape the different precipitation regimes. For instance, take the following examples:

- Between 1500 and 1800 UTC, the positive net area expansion (or net area increase) is clearly a dominant process over the continent; however, over the landside coast (region I), there is also a contribution from positive net initiation and positive advection to bring about the maximum FRAC values. This superposition would indicate, along with the occurrence of a higher merge (cf. previous section), the concurrent action of sea breeze and diurnal heating mechanisms.
- Over the seaside coast, between 0600 and 0900 UTC, positive net area expansion is the dominant process and is related to the early morning maximum precipitation in the seaside coastal regime. On the other hand, between 2100 and 0000 UTC, the dominant process for the FRAC decrease is not the net area expansion; it is the superposition between a negative net initiation and a negative advection.

In general, zonal advection is important close to coastal regions:

- Over the coastal region of Amapá between 2100 and 0000 UTC, there is a high level of similarity between the temporal variation pattern in the FRAC and that of zonal advection, which illustrates the importance of advective processes over the coast and the region of phase propagation between the coast and inland areas.
- Over northwestern Pará and northeastern Amazonas, there is a transition between the type 5 and type 6 regimes. The phase gradient does not indicate phase propagation during the late night to midmorning

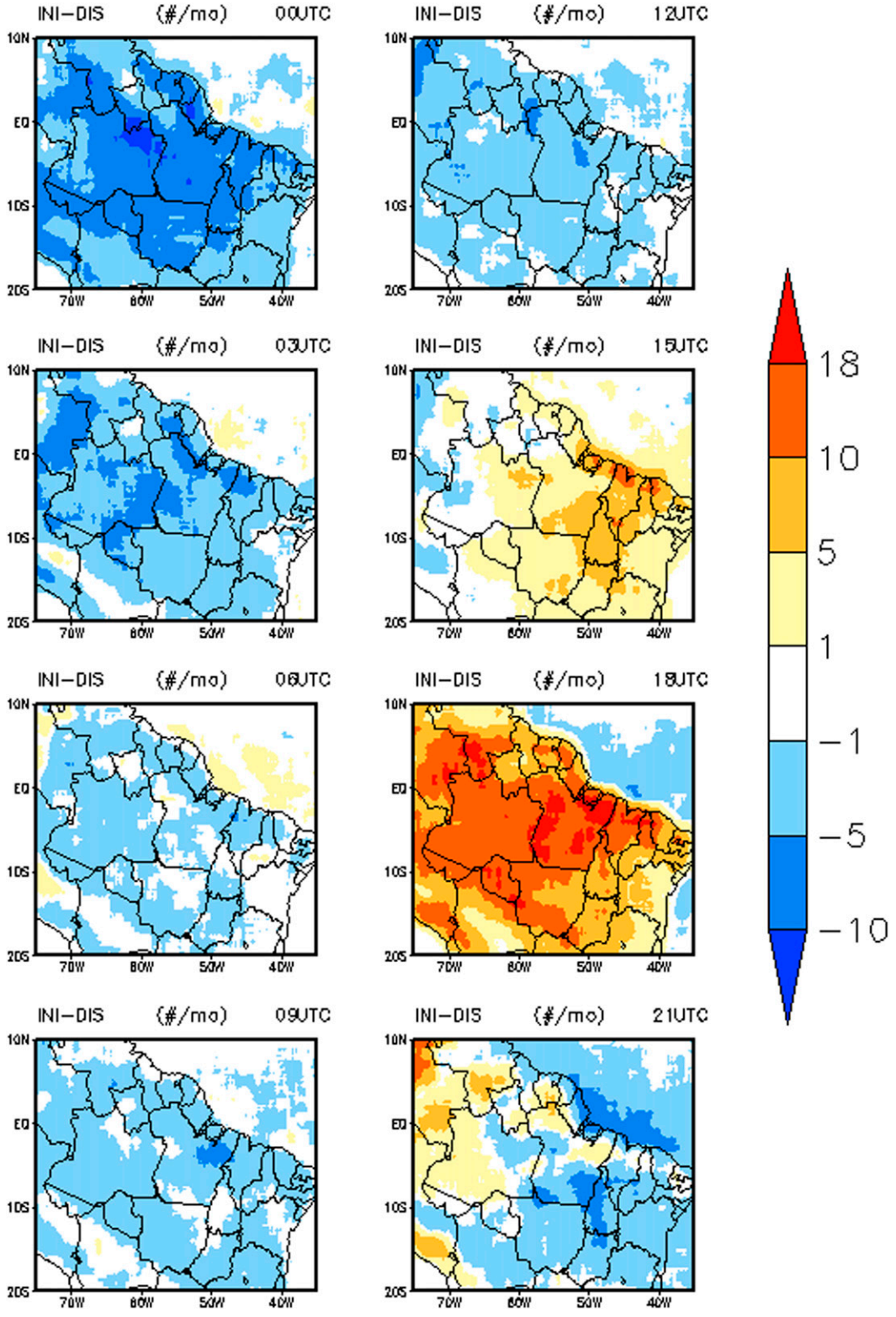

FIG. 12. Daily cycle frequency of the CS net initiation (initiation − dissipation).

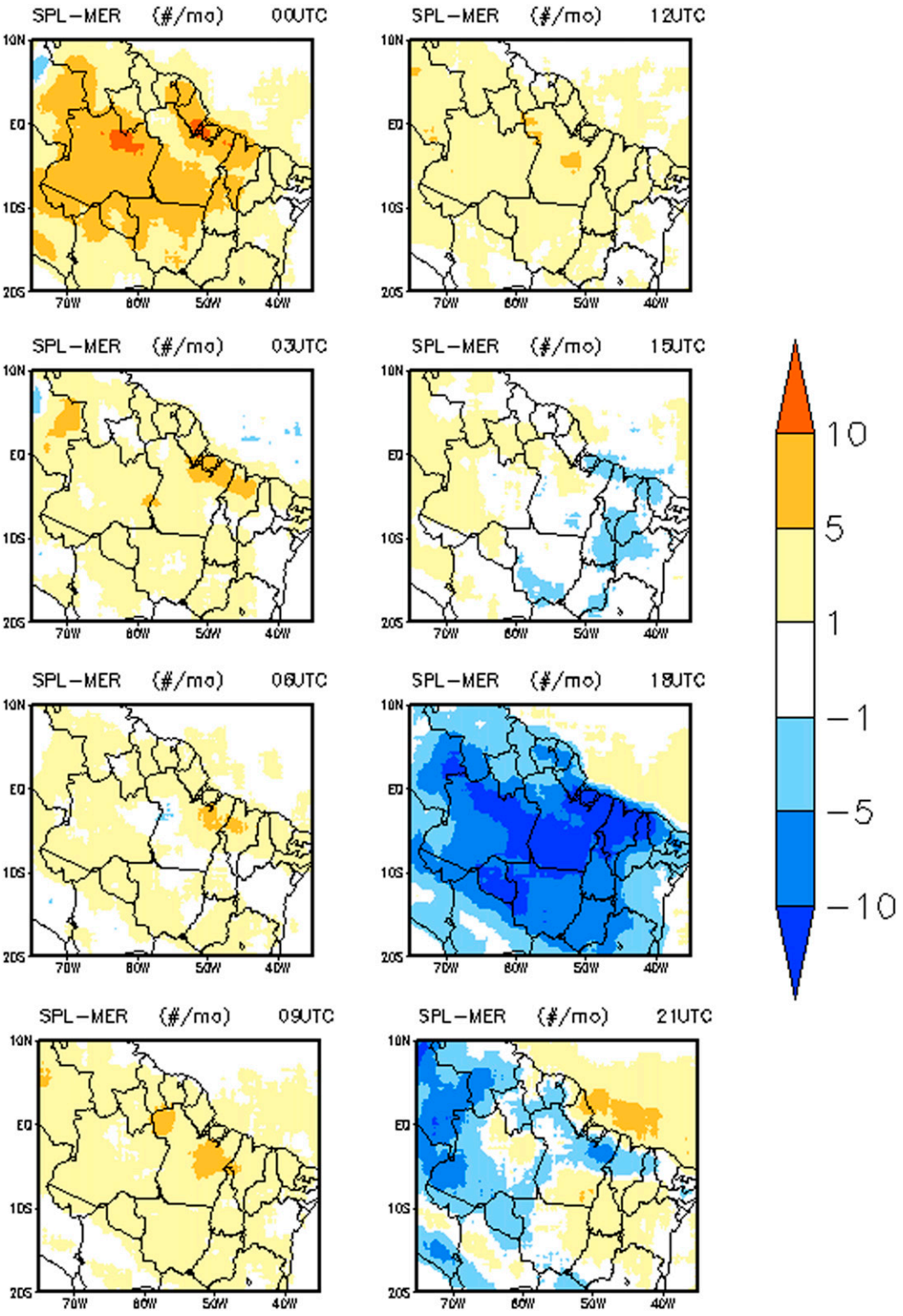

FIG. 13. Daily cycle frequency of the CS net split (split − merge).

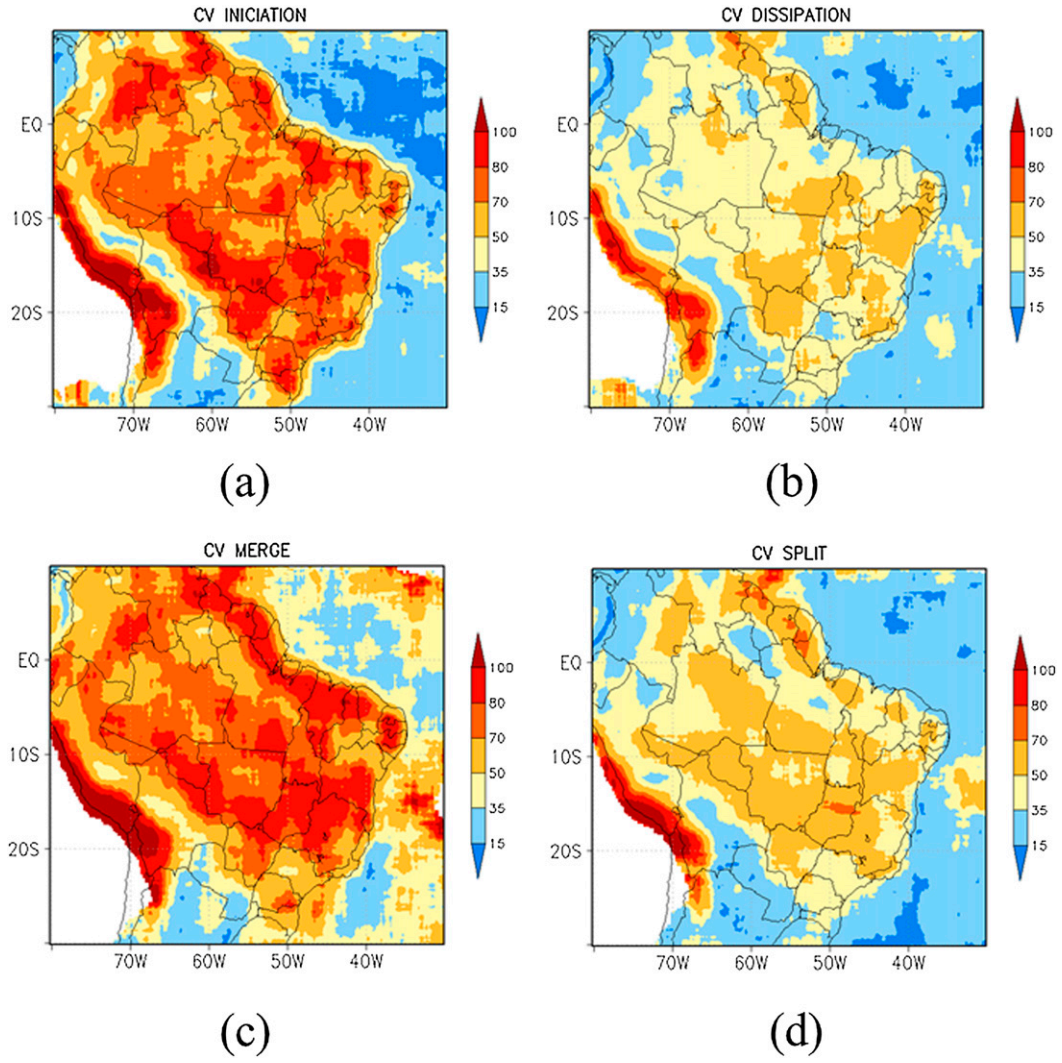

FIG. 14. Coefficient of variation for the (a) initiation, (b) dissipation, (c) merge, and (d) split.

(0300–1200 UTC); however, there is a strong positive advection that prevents the FRAC from decreasing.

From midnight to midday (from 0300 to 1500 UTC), the variations in the FRAC are small over the continent, resulting from the small magnitude of the net processes.

d. Convective systems related processes for contrasting regimes

The daily regime cycles can be grouped into continental and oceanic categories. In the oceanic regime, the temporal FRAC variations have a small magnitude, which explains the lower intradaily variability (Fig. 4). Over the day, net dissipation and small negative advection are observed; during the night and morning (from 0300–1500 UTC), these processes partially balance the net area increase; and in the late afternoon (2100 UTC), they act concurrently with the net area reduction, leading to a sharper decrease in the FRAC (Fig. 16). The daily average net area increase is balanced primarily by net dissipation and secondarily by negative advection.

The continental regimes, except type 3 (shore regime), could be grouped into coastal (types 4 and 5) and inland regimes (types 6 and 7). The main difference between these two groups is (Figs. 17, 18) the role of advection, which has higher (lower) magnitude during the day in the coastal (inland) regimes and a net area increase during the afternoon, which is higher (lower) in the coastal (inland) regimes. In the coastal regimes, advection and net area increase act concurrently to increase the magnitude of the temporal variations in the FRAC, which leads to higher intradaily variability.

The main difference between types 4 and 5 is the phase lag in the advection process (Fig. 19); in type 5, the

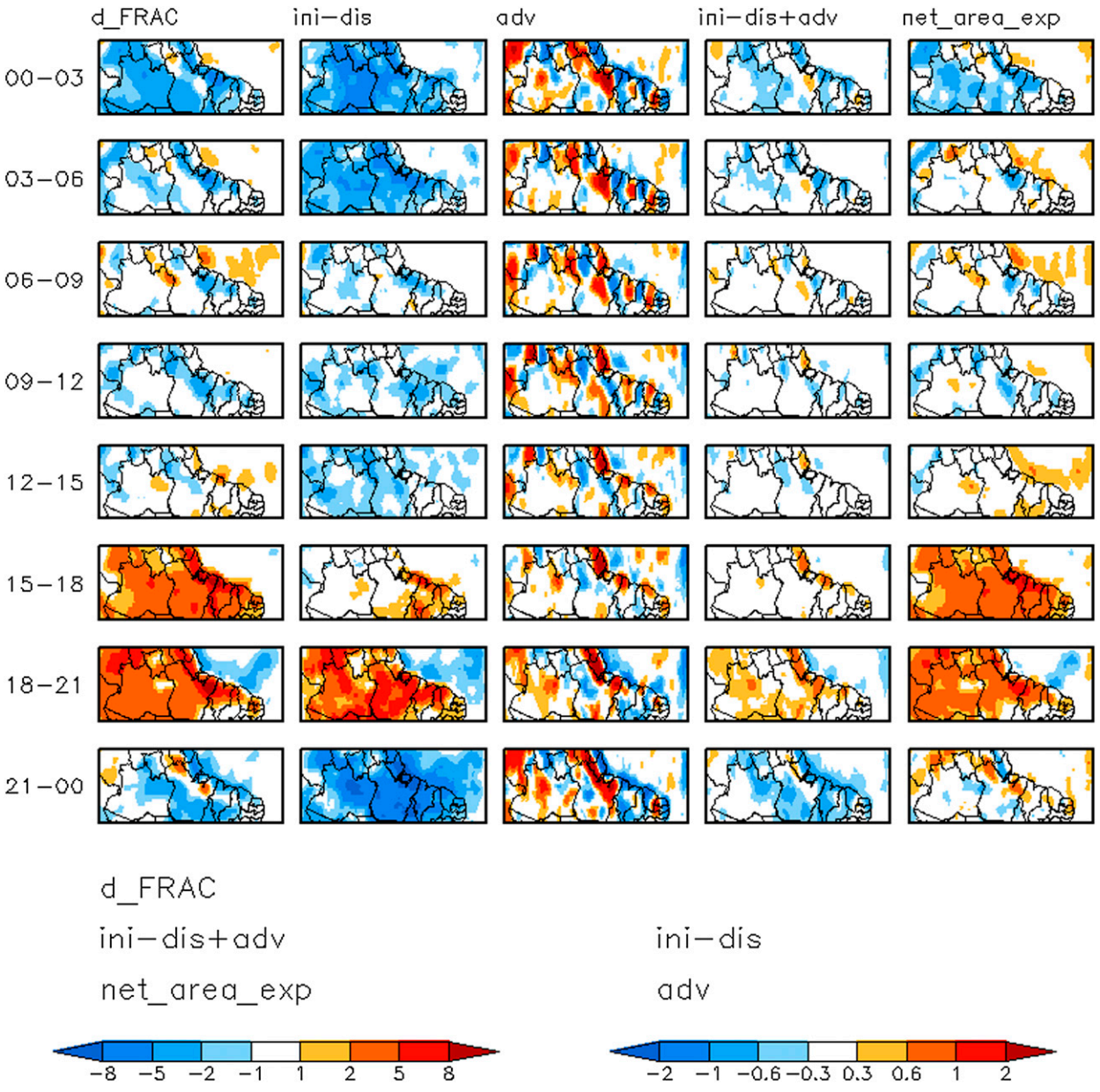

FIG. 15. Daily cycle of the FRAC temporal variation and its processes (net initiation, net expansion, and zonal advection).

positive (negative) advection has a maximum magnitude during the night (morning); in type 4, the positive (negative) advection has maximum magnitude during the afternoon (night).

The main difference between regimes 6 and 7 is the magnitude of the net area expansion (Fig. 20). In regime 7, the magnitude is higher for both the net area increase in the afternoon (1500–1800 and 1800–2100 UTC) and the net area reduction in the night/morning (from 0000–0300 to 0900–1200 UTC; particularly at 0000–0300 UTC, when the difference is higher). For the difference in the afternoon, the hypothesis is that, in type 7, there is re-intensification of the convection initiated over the coast in the previous day (e.g., region III). Other regional factors, such as the river breeze, may also contribute to the higher net area increase.

e. Modeling of the net area expansion

In general, as shown previously, the most important process that explains the FRAC temporal variations is the net area expansion of the CS. It has a well-defined and almost common daily cycle to all continental

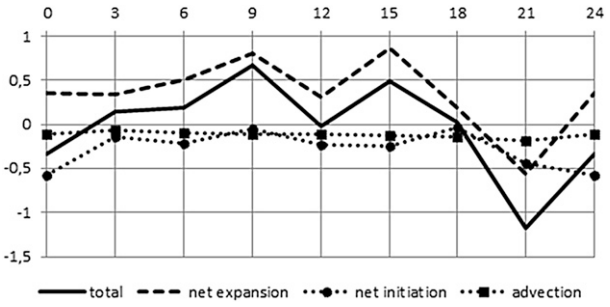

FIG. 16. Temporal FRAC variations of the oceanic regime (type 1) related to the net initiation, net expansion, and zonal advection processes.

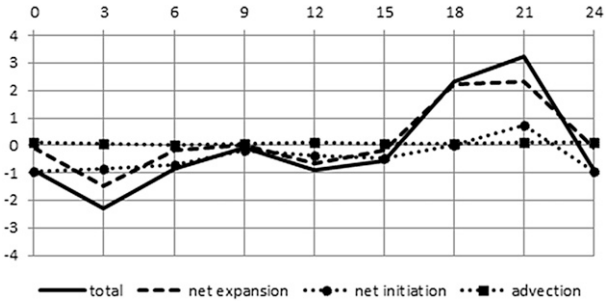

FIG. 18. As in Fig. 16, but for the inland regime (type 6).

regimes, with net area increase during the afternoon followed by net area reduction in the night and morning. To evaluate the two components of the net area expansion, it is assumed that the area increase is proportionate to the initiation [Eq. (10)]. The area decrease is obtained as a residual (i.e., net area expansion minus the area increase). The proportionality between the area increase and initiation embodies the idea that the physical mechanisms that favor initiation, such as diurnal solar heating, would also favor area expansion. This idea is based on the similarity between the daily cycle of CS initiation and the merge. For simplicity, the same constant of proportionality is prescribed for all regions (either continental or oceanic).

The area cycles increase in contrasting continental regimes, such as types 4 and 6, but are fairly similar, and the same holds for the area reduction cycles (Fig. 21). Therefore, advection is one of the main processes related to the difference between coastal and inland regimes. For type 4, the slightly higher maximum in the area increase cycle may be due to the sea breeze mechanism. For both regimes, the magnitude of area reduction shows an early night maximum (0000 UTC) and decays during the night, attaining an almost steady value during the morning.

One simple way to represent the area reduction consists of assuming that the FRAC decays exponentially in the absence of atmospheric area increase factors–mechanisms [Eq. (12)]. The exponential decay depends on one parameter, the *e*-folding time τ. The intradaily variability of τ is shown in Fig. 22. For both regimes, a maximum of τ is found at 2100 UTC; next, the afternoon maximum in area increases at 1800 UTC, and then the τ decays during the night and morning. The values of τ, which range in general between 6 and 12 h, indicate a slow decrease in the FRAC. This behavior may be due to the upscaling of the CS in mesoscale convective systems, whose lifetime is compatible with the values of τ (Cotton and Anthes 1989; Houze 1993; Machado et al. 1998; Barbosa et al. 2006).

By considering the occurrence of CS merge as a proxy for upscaling, it is found that considerable upscaling takes place over the continent in the afternoon (1800–2100 UTC). This means that the CS initiates, expands, and upscales over the continent in the afternoon. From the night until the following day's afternoon, there is progressive weakening of the upscaling organization and therefore a progressive reduction in τ. The values of τ, however, remain relatively high; it means that CS organization at larger scales continues, even undergoing some weakening.

Another way to represent the effect of upscaling in the time scale of CS decay consists of keeping τ fixed and equal to the value expected for the individual CS (such as a few hours) and adding an additional source of the

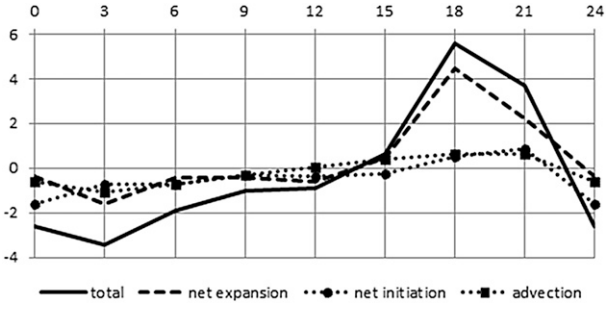

FIG. 17. As in Fig. 16, but for the coastal regime (type 4).

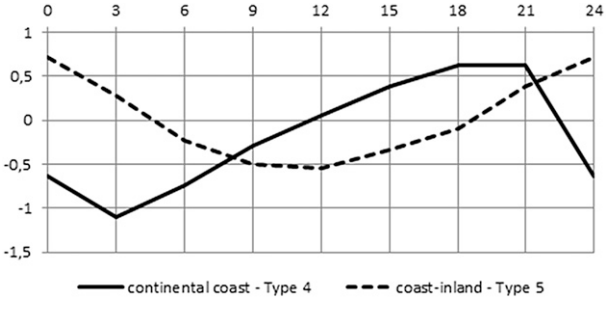

FIG. 19. Similar to Fig. 16, but for the continental coast regime (type 4) and the coastal inland regime (type 5).

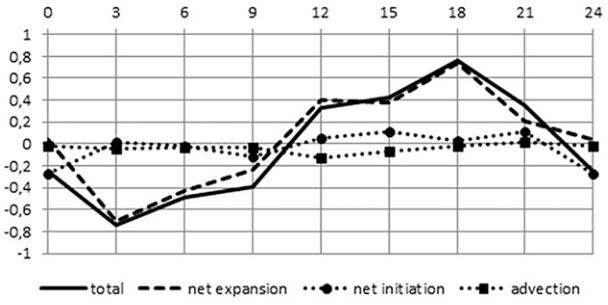

FIG. 20. As in Fig. 16, but for the type 7 minus type 6 regimes.

CS area increase depending on the upscaling degree. This representation is based on the autopropagation mechanism of mesoscale convective systems, by which the downdrafts of the CS included in the system merge and initiate new convective cells in the direction of the system propagation (Cotton and Anthes 1989). Under this representation, the CS embedded in large-scale systems decay slower than the isolated CS because part of the area reduction is balanced by the additional source.

6. Concluding remarks

In this work, the different regimes of the daily cycle of precipitation over the Brazilian northern coast during austral autumn were studied. The coefficient of variation, that is, the intradaily standard deviation divided by the daily average, was used as the primary measure of intradaily variability. The regimes proposed here build on those obtained by KW08.

The existence of a new regime, named the shore regime (type 3), was noticed. This regime exists over a narrow strip (width of ~1°) along the shore, where the minimum CV values are found, and its cycle shows two weak maxima: one in the morning, which is a seaside coastal feature; and the other in late afternoon, which is a continental feature. The region of the Alcântara Launch Center, for instance, would be under this regime. The features of this new regime need to be confirmed in future studies by using other datasets because there are uncertainties in the TRMM data along the shore areas due to the differences between TRMM algorithms over oceanic and continental regions. These studies could also address the convective systems processes that shape the regime's daily precipitation cycle; for this, novel methods to get CS information should be developed because of the narrowness of the shore regime location.

The landside coastal regime of KW08 was divided into two categories: the continental coast regime (type 4) and the coast–inland regime (type 5). These two regimes

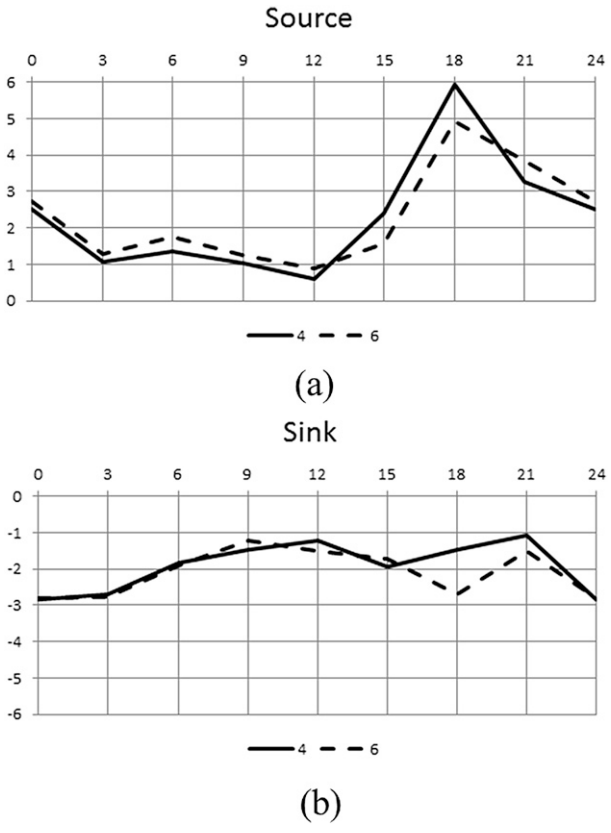

FIG. 21. Daily cycles of the CS area (a) increase (source) and (b) reduction (sink) for contrasting continental regimes (types 4 and 6).

show a nonuniform cycle and are located over the landside coast. In type 4, there are pronounced afternoon maximum and high CV values; in type 5, there is clear inland phase propagation, that is, the maximum of type 4 propagates inland during the night, and the CV decreases inland. For classification purposes, type 4 is 2° from the coastline, and type 5 is between 2° and 7°.

The intradaily variability over the large inland area (>7° far from the coastline) that includes well-known regions like central Amazonia would be better depicted by an alternating sequence of high- and low-variability

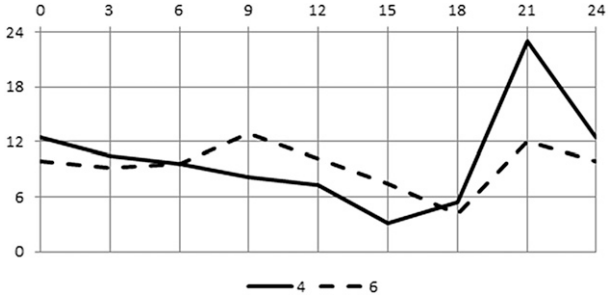

FIG. 22. Intradaily variability of τ or the time scale for the CS area reduction (h).

modes. Therefore, the continental regime of KW08 was divided into two categories: the low-variability inland regime (type 6) and the high-variability inland regime (type 7). In type 6, the CV is low and the cycle is quasi uniform with two weak maxima: one in the late afternoon due to diurnal solar radiation heating and the other in the early morning due to phase propagation and/or nocturnal convection processes. In type 7, variability is higher because of the more intense afternoon maximum (compared to type 6).

The daily cycle of the CS occurrence and processes was also studied. Strong agreement between the daily cycle of precipitation and the CS occurrence (frequency and area fraction) was found. This relationship is always assumed, and it was ratified here. The CS initiation (dissipation) is more concentrated (distributed) in time, and it is directly related to the CS merge (split). The similarity between the initiation and merge suggests that the physical mechanisms that favor initiation, such as the diurnal solar heating, also favor a CS area increase and subsequent merge.

At the first order, net area expansion (CS area increase minus decrease) is the main process of temporal variations in the area fraction covered by the CS (FRAC). Advection and net initiation processes are important for some regions/periods of time, and they contribute to shape the different daily cycle regimes proposed here.

The oceanic regime (type 1) shows smaller magnitude values of FRAC temporal variations, which are consistent with the very low intradaily variability of this regime. The net area increase is balanced primarily by net dissipation and secondarily by negative advection. Advection is an important process for the landside coastal regimes (types 4 and 5), and its phase is distinct for types 4 and 5. In the inland continental regimes (types 6 and 7), the role of advection is small and the slow decay of the CS area during the night and morning is an important feature.

By considering a simple parameterization—that the CS area increase is dependent on initiation—the time scale of CS area reduction under environmental conditions unfavorable to initiation (night–morning time) ranges from 6 to 12 h. This is compatible with the time scale/lifetime of CS organized on larger scales, such as mesoscale convective systems, and is much higher than the time scale/lifetime of individual (isolated) CS. Therefore, our results suggest that, during the afternoon, widespread upscaling of CS occurs over the continent concurrently with an intense CS area increase and merge. As the nighttime begins, isolated CS decay and dissipate rapidly. The remaining CS, which have undergone upscaling and are thus organized at a larger scale, decay slowly during the night and morning, leading to a more uniform cycle over inland areas. This integrated picture notes the key role of the upscaling processes on the daily cycle of precipitation.

Acknowledgments. This work is part of the first author's doctoral thesis under the guidance of the second author. The first author was supported by a grant from the National Council for Scientific and Technological Development (CNPq). The positive comments from two anonymous reviewers are gratefully acknowledged.

REFERENCES

Alcântara, C. R., M. A. F. Silva Dias, E. P. Souza, and J. C. P. Cohen, 2011: Verification of the role of the low level jets in Amazon squall lines. *Atmos. Res.,* **100,** 36–44, doi:10.1016/j.atmosres.2010.12.023.

Barbosa, R. L., M. D. Oyama, and L. A. T. Machado, 2006: Climatologia das perturbações convectivas iniciadas na costa norte do Brasil (Climatology of convective perturbations initiated on the north coast of Brazil). *Rev. Bras. Meteor.,* **21** (1), 107–117.

Barros, S. S., 2008: Precipitação no Centro de Lançamento de Alcântara: Aspectos observacionais e de modelagem (Precipitation in the Alcântara Launch Center: Observational and modeling aspects). M.Sc. thesis, Centro de Previsão de Tempo e Estudos Climáticos, Instituto Nacional de Pesquisas Espaciais, 112 pp.

Bowman, K. P., J. C. Collier, G. R. North, Q. Wu, E. Ha, and J. Hardin, 2005: Diurnal cycle of tropical precipitation in Tropical Rainfall Measuring Mission (TRMM) satellite and ocean buoy rain gauge data. *J. Geophys. Res.,* **110,** D21104, doi:10.1029/2005JD005763.

Brito, S. S. B., 2013: Ciclo diário de precipitação no norte do Brasil (Daily cycle of precipitation in northern Brazil). Ph.D. thesis, Instituto Nacional de Pesquisas Espaciais, 152 pp.

Cohen, J. C. P., M. A. F. Silva Dias, and C. A. Nobre, 1995: Aspectos climatológicos das linhas de instabilidade na Amazônia (Climatological aspects of squall lines in Amazonia). *Climanálise,* **4** (11), 34–40.

Cotton, W. R., and R. A. Anthes, 1989: *Storm and Cloud Dynamics.* Academic Press, 880 pp.

Cutrim, E. M. C., D. W. Martin, D. G. Butzow, I. M. Silva, and E. Yulaeva, 2000: Pilot analysis of hourly rainfall in central and eastern Amazonia. *J. Climate,* **13,** 1326–1334, doi:10.1175/1520-0442(2000)013<1326:PAOHRI>2.0.CO;2.

Garreaud, R. D., and J. M. Wallace, 1997: The diurnal march of convective cloudiness over the Americas. *Mon. Wea. Rev.,* **125,** 3157–3171, doi:10.1175/1520-0493(1997)125<3157:TDMOCC>2.0.CO;2.

Gonçalves, W. A., 2013: Uma avaliação do efeito dos aerossóis na organização e estrutura das nuvens convectivas (An evaluation of the effect of aerosols in organization and structure of convective clouds). Ph.D. thesis, Instituto Nacional de Pesquisas Espaciais, 155 pp.

Gray, W. M., and R. W. Jacobson Jr., 1977: Diurnal variation of deep cumulus convection. *Mon. Wea. Rev.,* **105,** 1171–1188, doi:10.1175/1520-0493(1977)105<1171:DVODCC>2.0.CO;2.

Houze, R. A., Jr., 1993: *Cloud Dynamics.* Academic Press, 573 pp.

Huffman, G. J., and Coauthors, 2007: The TRMM Multisatellite Precipitation Analysis (TMPA): Quasi-global, multiyear, combined-sensor precipitation estimates at fine scales. *J. Hydrometeor.,* **8,** 38–55, doi:10.1175/JHM560.1.

Janowiak, J. E., V. E. Kousky, and R. J. Joyce, 2005: Diurnal cycle of precipitation determined from the CMORPH high spatial and temporal resolution global precipitation analyses. *J. Geophys. Res.,* **110,** D23105, doi:10.1029/2005JD006156.

Jeong, J., A. Walther, G. Nikulin, D. Chen, and C. Jones, 2011: Diurnal cycle of precipitation amount and frequency in Sweden: Observation versus model simulation. *Tellus,* **63A,** 664–674, doi:10.1111/j.1600-0870.2011.00517.x.

Kikuchi, K., and B. Wang, 2008: Diurnal precipitation regimes in the global tropics. *J. Climate,* **21,** 2680–2696, doi:10.1175/2007JCLI2051.1.

Kousky, V. E., 1980: Diurnal rainfall variation in Northeast Brazil. *Mon. Wea. Rev.,* **108,** 488–498, doi:10.1175/1520-0493(1980)108<0488:DRVINB>2.0.CO;2.

Laurent, H., L. A. T. Machado, C. Morales, and L. Durieux, 2002: Characteristics of Amazonian mesoscale convective systems observed from satellite and radar during the WETAMC/LBA experiment. *J. Geophys. Res.,* **107,** 8054, doi:10.1029/2001JD000337.

Machado, L. A. T., and W. B. Rossow, 1993: Structural characteristics and radiative properties of tropical cloud clusters. *Mon. Wea. Rev.,* **121,** 3234–3260, doi:10.1175/1520-0493(1993)121<3234:SCARPO>2.0.CO;2.

——, ——, R. L. Guedes, and A. W. Walker, 1998: Life cycle variations of mesoscale convective systems over the Americas. *Mon. Wea. Rev.,* **126,** 1630–1654, doi:10.1175/1520-0493(1998)126<1630:LCVOMC>2.0.CO;2.

Mao, J. Y., and G. X. Wu, 2012: Diurnal variations of summer precipitation over the Asian monsoon region as revealed by TRMM satellite data. *Sci. China Earth Sci.,* **55,** 554–566, doi:10.1007/s11430-011-4315-x.

Nesbitt, S. W., and E. J. Zipser, 2003: The diurnal cycle of rainfall and convective intensity according to three years of TRMM measurements. *J. Climate,* **16,** 1456–1475, doi:10.1175/1520-0442-16.10.1456.

Rickenbach, T. M., 2004: Nocturnal cloud systems and the diurnal variation of clouds and rainfall in southwestern Amazonia. *Mon. Wea. Rev.,* **132,** 1201–1219, doi:10.1175/1520-0493(2004)132<1201:NCSATD>2.0.CO;2.

Sapiano, M. R. P., and P. A. Arkin, 2009: An intercomparison and validation of high-resolution satellite precipitation estimates with 3-hourly gauge data. *J. Hydrometeor.,* **10,** 149–166, doi:10.1175/2008JHM1052.1.

Silva, C. M. S., 2013: Ciclo diário e semidiário de precipitação na costa norte do Brasil (Daily and semidaily cycles of precipitation in the northern coast of Brazil). *Rev. Bras. Meteor.,* **28** (1), 34–42, doi:10.1590/S0102-77862013000100004.

Spiegel, M. R., 1978: *Probabilidade e estatística (Probability and Statistics)*. McGraw-Hill Brasil, 518 pp.

Teixeira, R. F. B., 2008: O fenômeno da brisa e sua relação com a chuva sobre Fortaleza-CE (The breeze phenomenon and its relationship with rain on Fortaleza-CE). *Rev. Bras. Meteor.,* **23** (3), 282–291, doi:10.1590/S0102-77862008000300003.

Turk, F. J., P. Arkin, M. R. P. Sapiano, and E. E. Ebert, 2008: Evaluating high-resolution precipitation products. *Bull. Amer. Meteor. Soc.,* **89,** 1911–1916, doi:10.1175/2008BAMS2652.1.

Velasco, I., and J. M. Fritsch, 1987: Mesoscale convective complexes in the Americas. *J. Geophys. Res.,* **92,** 9591–9613, doi:10.1029/JD092iD08p09591.

Vila, D. A., L. A. T. Machado, H. Laurent, and I. Velasco, 2008: Forecast and Tracking the Evolution of Cloud Clusters (ForTraCC) using satellite infrared imagery: Methodology and validation. *Wea. Forecasting,* **23,** 233–245, doi:10.1175/2007WAF2006121.1.

Wallace, J. M., and P. V. Hobbs, 2006: *Atmospheric Science: An Introductory Survey.* Academic Press, 488 pp.

Wilks, D. S., 2006: *Statistical Methods in the Atmospheric Sciences.* 2nd ed. Academic Press, 627 pp.

Yang, G. Y., and J. Slingo, 2001: The diurnal cycle in the tropics. *Mon. Wea. Rev.,* **129,** 784–801, doi:10.1175/1520-0493(2001)129<0784:TDCITT>2.0.CO;2.

Yang, S., and E. A. Smith, 2006: Mechanisms for diurnal variability of global tropical rainfall observed from TRMM. *J. Climate,* **19,** 5190–5226, doi:10.1175/JCLI3883.1.

Zhou, T., R. Yu, H. Chen, A. Dai, and Y. Pan, 2008: Summer precipitation frequency, intensity, and diurnal cycle over China: A comparison of satellite data with rain gauge observations. *J. Climate,* **21,** 3997–4010, doi:10.1175/2008JCLI2028.1.